UNDERWATER GLIDER DYNAMICS AND CONTROL *

Joshua G. Graver and Naomi Ehrich Leonard
Department of Mechanical & Aerospace Engineering
Princeton University
jggraver@princeton.edu, naomi@princeton.edu

12th International Symposium on Unmanned Untethered Submersible Technology, 2001

Abstract

We present a linear controller and observer design for autonomous underwater gliders based on a model of glider dynamics that we have derived. Our focus is on buoyancy-propelled, fixed-wing gliders with attitude controlled by means of internal mass distribution. In cases when some states cannot be directly measured, such as with oceangoing gliders, the design of an observer offers possible improvements over current glider control methods.

1 Introduction

Initially conceived by Henry Stommel [16], autonomous underwater gliders offer many advantages in ocean sensing: superior spatial and temporal measurement density, longer duration missions and greater operational flexibility. Several oceangoing gliders are operational or under development, including the SLOCUM glider [18], the "Spray" glider [14] and the "Seaglider" [3]. These are all buoyancy-propelled, fixed-winged gliders which shift internal ballast to control attitude.

On SLOCUM, the ballast tanks are configured within the vehicle to provide the proper pitching moment during upwards and downwards glides [17, 18]. A sliding battery mass is used for fine adjustments in pitch and roll. Sensors measure depth, pitch, roll, and compass heading. Vehicle position at the surface is determined through GPS fix. The pitch angle, an assumed angle of attack, and a vertical speed computed from depth measurements are used to estimate the horizontal speed of the glider. The glider control system periodically checks the glider attitude and adjusts the position of the sliding battery mass. Switching between downwards and upwards glides is performed open loop, i.e., the ballast is changed and the sliding mass is moved to a new position.

Sensing and control on other gliders is similar. For example, Spray performs active control of pitch and roll every 40 s using measured pitch and heading errors. In the case of pitch, a low-gain proportional control law is used, and in the case of heading, proportional plus integral control is used [14].

The goal of our work is to improve upon currently implemented glider control strategies. Our aim is to develop a widely applicable approach, complementing efforts on SLOCUM, Spray and Seaglider. Toward that end we have developed a nonlinear glider dynamic model and examined the use of linear controllers and observers. A model-based approach may also prove useful in determining optimal glider motions (see [2] for early work in this direction). Our glider dynamic model is derived in [10], where we examine steady glides, controllability and observability in the vertical plane.

In this paper we review the derivation from [10] and present a controller design that uses a linear observer. Because of space and power constraints, and because of the difficulties of underwater sensing, many operational gliders do not carry the sensors necessary to determine the full glider dynamic state. In particular, glider position and velocity are costly to measure directly. We design a dynamic observer to estimate the glider state from a limited set of measurements. These estimated states can be used to determine horizontal glider motion instead of the current methods which rely on assumptions of constant angle of attack.

Our dynamic glider model describes a glider with

*Research partially supported by the Office of Naval Research under grants N00014-98-1-0649 and N00014-01-1-0526 and by the National Science Foundation under grant BES-9502477.

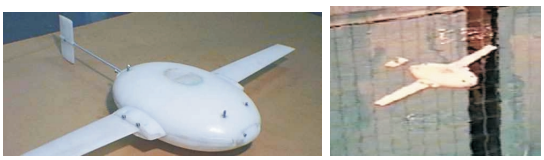

Figure 1.1: Experimental, laboratory-scale underwater glider ROGUE.

simple body and wing shape. Control is applied to two point masses inside the vehicle: we control the mass of a point with fixed position and the forces on a mass with variable position. The model describes the nonlinear coupling between the vehicle and the shifting and changing mass. Analysis and control law design is performed for the dynamics specialized to the vertical plane.

In related work with colleagues, we address issues in optimal path planning for underwater gliders [2] and in coordinating control for a network of autonomous underwater vehicles [1, 9, 15].

In Section 2 we describe our laboratory-scale glider ROGUE, see Figure 1.1. ROGUE controls buoyancy and CG position by means of a distributed array of independently actuated ballast tanks (syringes). In Section 3, we derive the equations of motion for a buoyancy-driven, fixed-wing underwater glider. Controllability and observability of steady glide paths in the vertical plane are studied in Section 4. Linear observers and linear control laws are developed in Section 5 for stabilizing these glide paths in the presence of disturbances. A simulation of the controlled glider modelled to resemble ROGUE is also presented. We give final remarks in Section 6.

2 The ROGUE gliding vehicle

ROGUE is a laboratory-scale gliding vehicle designed for experiments in glider dynamics and control. The vehicle consists of a water-tight body, modular wings and tail, internal ballast actuators, and on-board electronics and batteries. Using its on-board computer and sensors the vehicle is capable of autonomous or remote operation. ROGUE's ellipsoidal body has axes of length 18, 12 and 6 inches. The vehicle body contains the vehicle actuators, power, computer and sensors, and has mounts for the modular vehicle wings and tail. Different sets of wings and tail can be attached to perform experiments with different vehicle hydrodynamic profiles. We note that the body and wings have not been designed for optimal gliding performance but rather in consideration of available facilities and other manufacturing constraints. Experiments are currently planned using the ROGUE vehicle in our twenty-one-foot diameter laboratory tank and in an olympic sized pool at Princeton University.

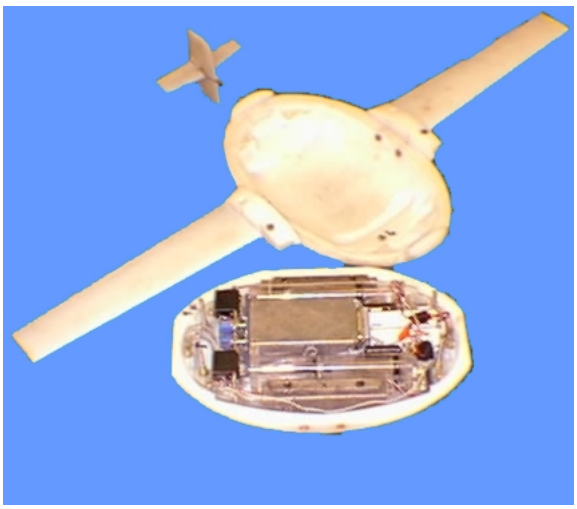

Figure 2.1: ROGUE with hull open.

In the configuration shown in Figure 2.1, each wing has span of 28 inches with aspect ratio 9.3. The wings are symmetric airfoils from [13] for low Reynolds number. The tail was sized using standard aircraft rules as in [4] and [11] . The vertical tail is designed to give yaw stability in forward glides and is modular, allowing tail volume to be changed. The glider body, wings and tail are all machined from UHMW (ultra-high molecular weight) plastic. In Figure 2.1 the top half of the vehicle is separated from the bottom so the internal components are visible. The metal box at the center of the vehicle contains the vehicle on-board computer. Two syringe-type ballast tanks are visible, one on each side of the computer housing. Visible to the left of each ballast tank is its driving servo (they appear as black squares). To the right of the computer housing are two white battery packs.

ROGUE contains three Nickel-Cadmium battery packs to provide power to the vehicle actuators, computer and sensors. Two "8-packs" of AA batteries power the computer, sensors and signal conditioning electronics. A "4-pack" of AA batteries powers the servos and vehicle optional R/C receiver.

ROGUE contains four independently actuated syringe-style ballast tanks aligned along the vehicle long axis, two mounted on each side of the vehicle centerline. The two ballast tanks in the upper half of the vehicle point forwards, while the two in the lower half point to the aft of the vehicle. Each tank

is made of a clear plastic cylinder with an internal plunger. Ball screw mechanisms with a high torque modified RC servo drive each ballast tank. The tank connects to the vehicle exterior via tubing. Moving the plunger inside each ballast tank transfers water from the tank to outside the vehicle or the reverse. Filling the tanks with different amounts of water causes ROGUE to become positively or negatively buoyant and moves the CG relative to the vehicle centroid. Each tank has a 100 mL capacity for .4" of plunger travel. Together the four tanks have a 400 g capacity. The relative positions of the four tanks allows for moderate adjustments in the vehicle CG position. The high torque servos driving the plungers connect to linear potentiometers and use feedback control to regulate the tank's plunger position. The tanks are filled completely with water before ROGUE is deployed to eliminate any air bubbles in the tanks.

ROGUE's on-board computer is a TattleTale Model 8. The TattleTale Model 8 is based on the Motorola 68332 chip and also includes a PIC 16C64 chip for low-power operation. The TattleTale allows up to 8 analog inputs and up to 25 digital input/output signals. The Motorola 68332 chip contains a central processor as well as a "time processing unit (TPU)" capable of performing simple clock functions independently of the main processor. There are 12 TPU channels available to the TattleTale user, each of which can generate a clock signal, measure the duty cycle of a square wave signal, etc. Electronics have been added to multiplex the analog input signals doubling the computer's analog input capacity to 16 channels. The TattleTale Model 8 includes 256 kilobytes of RAM (temporary memory) and 256 kilobytes of flash EEPROM (permanent memory). The memory can be expanded to any size available on a PCMCIA memory expansion card.

ROGUE's computer serves three major purposes: to store sensor data, process sensor data according to a pre-defined feedback control law, and apply command signals to ROGUE's actuators according to a feedback control law or to a remote command from a modified R/C transmitter.

TattleTale programs are written in C and compiled on a host computer. Programs may be downloaded from PC to TattleTale via serial link to the RAM or to EEPROM. The TattleTale is housed within a metal box to shield it from interference. Also mounted within the metal box is an optional R/C receiver for remote operation of the vehicle.

ROGUE's sensor suite includes the following elements: two depth sensors, two single-axis inclinometers mounted to measure pitch and roll angles, and three angular rate sensors mounted to measure pitch, roll and yaw rates. The vehicle also contains analog preamplifiers for each of the sensors. The amplifiers and angular sensors are mounted in a metal box in the lower half of the vehicle. The two pressure sensors are differential wet/wet sensors located at the fore and aft of the vehicle hull and are connected to the vehicle exterior and interior by tubing. The pressure sensors are used to measure depth. All sensors are connected to the on-board computer for logging data and performing feedback control using sensor data.

3 Glider Dynamics

The variables used in this paper are defined in Table 3.1.

Name	Description
α	angle of attack, $\cos\alpha = v_1/\sqrt{v_1^2+v_3^2}$
$\boldsymbol{b}$	vehicle position vector from inertial frame
CB	center of buoyancy and origin of body frame
CG	center of gravity
D	drag force
$\boldsymbol{D_f}$	added mass cross term
$\boldsymbol{F_{ext}}$	external force on vehicle in body coordinates
$\boldsymbol{f_{ext}}$	external force on vehicle in inertial coordinates
$\boldsymbol{\mathcal{I}}$	identity matrix
I	total mass/inertia matrix of vehicle/fluid system
$\boldsymbol{J_f}$	added inertia matrix
$\boldsymbol{J_h}$	inertia of the hull (excludes inertia due $\bar{m}$, m_w)
$\boldsymbol{J_s}$	inertia of stationary mass, $\boldsymbol{J_s} = \boldsymbol{J_h} - m_w\hat{\boldsymbol{r}}_{\boldsymbol{w}}\hat{\boldsymbol{r}}_{\boldsymbol{w}}$
$\boldsymbol{J}$	$\boldsymbol{J_s} + \boldsymbol{J_f}$
J_i	ith diagonal element of $\boldsymbol{J}$
$\boldsymbol{k}$	unit vector in direction of gravity
L	lift force
$\boldsymbol{M}$	sum of body and added mass, $\boldsymbol{M} = m_s\boldsymbol{\mathcal{I}} + \boldsymbol{M_f}$
$\boldsymbol{M_f}$	added mass matrix
M_{DL}	viscous moment
m	mass of displaced fluid
$\bar{m}$	movable point mass
m_b	variable ballast mass located at CB
m_{fi}	ith diagonal element of $\boldsymbol{M_f}$
m_i	ith diagonal element of $\boldsymbol{M}$
m_h	uniformly distributed hull mass
m_s	stationary body mass, $m_s = m_h + m_w + m_b$
m_v	total vehicle mass, $m_v = m_s + \bar{m}$
m_w	point mass for nonuniform hull mass distribution
m_0	excess mass, $m_0 = m_v - m$
$\boldsymbol{\Omega}$	angular velocity in body coordinates
Ω_i	ith component of $\boldsymbol{\Omega}$
$\boldsymbol{P}$	total linear momentum in body coordinates
$\boldsymbol{P_p}$	linear momentum of $\bar{m}$ in body coordinates
$\boldsymbol{\Pi}$	total angular momentum (body frame)
$\boldsymbol{R}$	rotation matrix for vehicle orientation
$\boldsymbol{r_P}$	position of movable mass $\bar{m}$ in body coordinates
r_{Pi}	ith component of $\boldsymbol{r_P}$
$\boldsymbol{r_s}$	position vector from CB to center of mass m_s
$\boldsymbol{r_w}$	position vector from CB to m_w
θ	pitch angle
$\boldsymbol{T_{ext}}$	total external torque in body coordinates
$\boldsymbol{\tau_{ext}}$	pure external torque in inertial coordinates
T	total kinetic energy, $T = T_s + T_p + T_f$
T_f	kinetic energy of fluid
T_p	kinetic energy of movable point mass
T_s	kinetic energy of stationary body mass m_s
$\vec{\boldsymbol{u}}$	$(u_1\ u_2\ u_3)^T$, force on sliding point mass
$\boldsymbol{u}$	$(u_1\ u_2\ u_3\ u_4)^T$, vector of control inputs
u_4	controlled variable mass rate, $u_4 = \dot{m}_b$
V	speed in vertical plane, $V = \sqrt{(v_1^2+v_3^2)}$
V_d	desired speed in vertical plane
$\boldsymbol{v}$	velocity in body coordinates
v_i	ith component of $\boldsymbol{v}$
x, y, z	components of vehicle position vector $\boldsymbol{b}$
ξ	glide path angle, $\xi = \theta - \alpha$
ξ_d	desired glide path angle
z'	perpendicular distance to desired glide path
z'_{ded}	dead reckoned value of z'

Table 3.1: Definition of variables.

3.1 Equations of Motion in 3D

We first review the derivation of the equations of motion for our underwater glider. For a more detailed derivation see [10]. Our choice of glider body and wing configuration is motivated by the designs of ROGUE, SLOCUM, Spray and Seaglider. We model the underwater glider as a rigid body with fixed wings (and tail) immersed in a fluid with buoyancy control and controlled internal moving mass. We take the hull to be ellipsoidal with wings and tail attached so that the center of buoyancy (CB) is at the center of the ellipsoid. We assign a coordinate frame fixed on the vehicle body to have its origin at the CB and its axes aligned with the principle axes of the ellipsoid. Let body axis 1 lie along the long axis of the vehicle (positive in the direction of the nose of the glider), let body axis 2 lie in the plane of the wings and body axis 3 point in the direction orthogonal to the wings as shown in Figure 3.1.

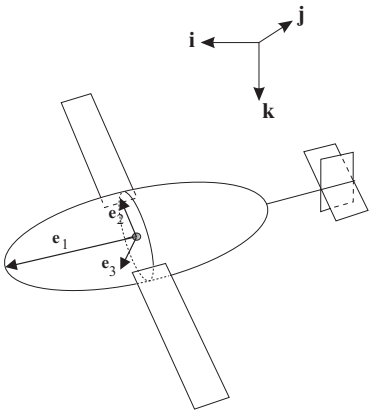

Figure 3.1: Frame assignment on underwater glider.

The total stationary mass, m_s, (also referred to as body mass) is the sum of three terms: m_h is a fixed mass that is uniformly distributed throughout the ellipsoid, m_w is a fixed point mass that may be offset from the CB, and m_b is the variable ballast point mass which is fixed in location at the CB. The vector from the CB to the point mass m_w is $\boldsymbol{r_w}$. The vector from the CB to the center of mass of the stationary mass $m_s = m_h + m_w + m_b$ is $\boldsymbol{r_s}$.

The moving internal point mass is $\bar{m}$. The vector $\boldsymbol{r_p}(t)$ describes the position of this mass with respect to the CB at time t. The total mass of the vehicle is then

$$m_v = m_h + m_w + m_b + \bar{m} = m_s + \bar{m}.$$

The mass of the displaced fluid is denoted m and we define $m_0 = m_v - m$ so that the vehicle is negatively (positively) buoyant if $-m_0$ is negative (positive). The different masses and position vectors are illustrated in Figure 3.2.

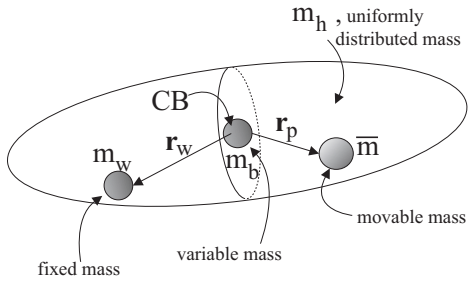

Figure 3.2: Glider mass definitions.

Let $\boldsymbol{J_h}$ denote the inertia matrix, with respect to the body frame, for the uniformly distributed mass m_h. Define the operator $\hat{}$ so that for a vector $\boldsymbol{x} = (x_1, x_2, x_3)^T$,

$$\hat{\boldsymbol{x}} = \begin{pmatrix} 0 & -x_3 & x_2 \\ x_3 & 0 & -x_1 \\ -x_2 & x_1 & 0 \end{pmatrix}.$$

Equivalently, for vector $\boldsymbol{y} = (y_1, y_2, y_3)^T$, $\hat{\boldsymbol{x}}\boldsymbol{y} = \boldsymbol{x} \times \boldsymbol{y}$. The inertia matrix for the stationary (body) mass expressed with respect to body frame coordinates is

$$\boldsymbol{J_s} = \boldsymbol{J_h} - m_w \hat{\boldsymbol{r}}_{\boldsymbol{w}} \hat{\boldsymbol{r}}_{\boldsymbol{w}}.$$

Since the variable ballast mass m_b is a point mass located at the CB, it does not contribute to $\boldsymbol{J_s}$, and in particular $\boldsymbol{J_s}$ is a constant.

The orientation of the glider is given by the rotation matrix $\boldsymbol{R}$. $\boldsymbol{R}$ maps vectors expressed with respect to the body frame into inertial frame coordinates. The position of the glider $\boldsymbol{b} = (x, y, z)^T$ is the vector from the origin of the inertial frame to the origin of the body frame (vehicle CB) as shown in Figure 3.3. The vehicle moves through the fluid with translational velocity $\boldsymbol{v} = (v_1, v_2, v_3)^T$ and angular velocity $\boldsymbol{\Omega} = (\Omega_1, \Omega_2, \Omega_3)^T$, expressed with respect to the body frame. (Note that we have diverged from the notation typical of the submarine literature where $\boldsymbol{v} = (u, v, w)^T$ and $\boldsymbol{\Omega} = (p, q, r)^T$. The notation that we use here is taken from texts in classical mechanics such as [5] and is more convenient for the derivation and analysis.) In this notation, the kinematics of the glider are given by

$$\dot{\boldsymbol{R}} = \boldsymbol{R}\hat{\boldsymbol{\Omega}} \quad (3.1)$$

$$\dot{\boldsymbol{b}} = \boldsymbol{R}\boldsymbol{v}. \quad (3.2)$$

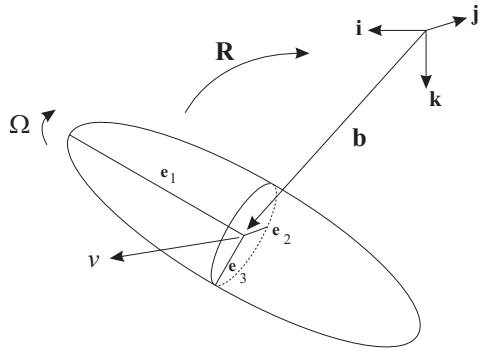

Figure 3.3: Glider position and orientation variables.

Let $\boldsymbol{P}$ be the momentum of the vehicle-fluid system expressed with respect to the body frame. Let $\boldsymbol{\Pi}$ be the total angular momentum about the origin of the body frame. Let $\boldsymbol{P_p}$ represent the point mass momentum with respect to the body frame. We differentiate the expressions relating the momenta $\boldsymbol{P}$, $\boldsymbol{\Pi}$, and $\boldsymbol{P_p}$ to the momenta in the inertial frame. Applying the kinematic expressions (3.2) and (3.1), then applying Newton's laws, gives the following dynamic equations in body coordinates:

$$\dot{\boldsymbol{P}} = \boldsymbol{P} \times \boldsymbol{\Omega} + \boldsymbol{R}^T \sum_{i=1}^{I} \boldsymbol{f_{ext_i}}, \tag{3.3}$$

$$\begin{aligned} \dot{\boldsymbol{\Pi}} &= \boldsymbol{\Pi} \times \boldsymbol{\Omega} + \boldsymbol{P} \times \boldsymbol{v} \\ &+ \boldsymbol{R}^T \left(\sum_{i=1}^{I} (\boldsymbol{x_i} - \boldsymbol{b}) \times \boldsymbol{f_{ext_i}} \right) + \boldsymbol{R}^T \sum_{j=1}^{J} \boldsymbol{\tau_{ext_j}}, \end{aligned} \tag{3.4}$$

$$\dot{\boldsymbol{P}}_{\boldsymbol{p}} = \boldsymbol{P_p} \times \boldsymbol{\Omega} + \bar{m} g (\boldsymbol{R}^T \boldsymbol{k}) + \tilde{\boldsymbol{u}}, \tag{3.5}$$

where all vectors are expressed with respect to the inertial frame. The vector $\boldsymbol{x_i}$ locates the point of application of the force $\boldsymbol{f_{ext_i}}$ with respect to the inertial coordinate frame. $\boldsymbol{f_{ext_i}}$ is an external force applied to the system and $\boldsymbol{\tau_{ext_j}}$ is a pure external torque. $\boldsymbol{k}$ is a unit vector pointing in the direction of gravity. These external forces and torques include those due to gravity and buoyancy; however, gravity is included explicitly in the third set of equations as it is the only external force acting on the movable point mass. $\tilde{\boldsymbol{u}} = \boldsymbol{R}^T \sum_{k=1}^{K} \boldsymbol{f_{int_k}}$ is the internal force applied from the vehicle body onto the point mass (a control force) in body coordinates.

Define the control vector

$$\bar{\boldsymbol{u}} = \begin{pmatrix} u_1 \\ u_2 \\ u_3 \end{pmatrix} = \dot{\boldsymbol{P}}_{\boldsymbol{p}} = \boldsymbol{P_p} \times \boldsymbol{\Omega} + \bar{m} g (\boldsymbol{R}^T \boldsymbol{k}) + \tilde{\boldsymbol{u}}. \tag{3.6}$$

To derive expressions for $\boldsymbol{P}$, $\boldsymbol{\Pi}$, and $\boldsymbol{P_p}$, we determine the total kinetic energy of the glider-fluid system. Let T_s be the kinetic energy of the rigid body with mass m_s and inertia matrix $\boldsymbol{J_s}$. Let $\boldsymbol{v_p}$ be the absolute velocity of the movable point mass $\bar{m}$ expressed in body coordinates. Given that the velocity of $\bar{m}$ relative to the body frame is $\dot{\boldsymbol{r}}_{\boldsymbol{p}}$, we compute

$$\boldsymbol{v_p} = \boldsymbol{v} + \dot{\boldsymbol{r}}_{\boldsymbol{p}} + \boldsymbol{\Omega} \times \boldsymbol{r_p} \ . \tag{3.7}$$

The kinetic energy T_p of the movable point mass is then computed to be

$$T_p = \frac{1}{2} \bar{m} \|\boldsymbol{v_p}\|^2 \ .$$

Kirchhoff [8] showed that the kinetic energy of an unbounded volume of ideal fluid due to the motion of an immersed rigid body takes the form

$$T_f = \frac{1}{2} \begin{pmatrix} \boldsymbol{v} \\ \boldsymbol{\Omega} \end{pmatrix} \cdot \begin{pmatrix} \boldsymbol{M_f} & \boldsymbol{D_f^T} \\ \boldsymbol{D_f} & \boldsymbol{J_f} \end{pmatrix} \begin{pmatrix} \boldsymbol{v} \\ \boldsymbol{\Omega} \end{pmatrix}, \tag{3.8}$$

where $\boldsymbol{M_f}$ is the added mass matrix, $\boldsymbol{J_f}$ is the added inertia matrix and $\boldsymbol{D_f}$ is the added cross term. These matrices depend upon the external shape of the body and the density of the fluid. We assume that at low angle of attack, the contribution of the wings is dominated by lift and drag forces. Thus, we make the simplifying assumption that the added mass and inertia terms can be computed solely from the vehicle hull.

The total vehicle fluid kinetic energy $T = T_s + T_p + T_f$ is computed to be

$$T = \frac{1}{2} \begin{pmatrix} \boldsymbol{v} \\ \boldsymbol{\Omega} \\ \dot{\boldsymbol{r}}_{\boldsymbol{p}} \end{pmatrix} \cdot \boldsymbol{I} \begin{pmatrix} \boldsymbol{v} \\ \boldsymbol{\Omega} \\ \dot{\boldsymbol{r}}_{\boldsymbol{p}} \end{pmatrix},$$

Where $\boldsymbol{I} =$

$$\begin{pmatrix} (m_s + \bar{m})\boldsymbol{\mathcal{I}} + \boldsymbol{M_f} & -\bar{m}\hat{\boldsymbol{r}}_{\boldsymbol{p}} - m_s \hat{\boldsymbol{r}}_{\boldsymbol{s}} + \boldsymbol{D_f^T} & \bar{m}\boldsymbol{\mathcal{I}} \\ \bar{m}\hat{\boldsymbol{r}}_{\boldsymbol{p}} + m_s \hat{\boldsymbol{r}}_{\boldsymbol{s}} + \boldsymbol{D_f} & \boldsymbol{J_s} - \bar{m}\hat{\boldsymbol{r}}_{\boldsymbol{p}}\hat{\boldsymbol{r}}_{\boldsymbol{p}} + \boldsymbol{J_f} & \bar{m}\hat{\boldsymbol{r}}_{\boldsymbol{p}} \\ \bar{m}\boldsymbol{\mathcal{I}} & -\bar{m}\hat{\boldsymbol{r}}_{\boldsymbol{p}} & \bar{m}\boldsymbol{\mathcal{I}} \end{pmatrix}.$$

Since the vehicle hull is ellipsoidal (we neglect the wings in this instance), $\boldsymbol{M_f}$ and $\boldsymbol{J_f}$ are diagonal and $\boldsymbol{D_f} = \boldsymbol{0}$. Let $\boldsymbol{M_f} = \mathrm{diag}(m_{f1}, m_{f2}, m_{f3})$ and $\boldsymbol{J_f} = \mathrm{diag}(J_{f1}, J_{f2}, J_{f3})$. Define

$$\boldsymbol{M} = m_s \boldsymbol{\mathcal{I}} + \boldsymbol{M_f}, \quad \boldsymbol{J} = \boldsymbol{J_s} + \boldsymbol{J_f},$$

where $\boldsymbol{\mathcal{I}}$ is the 3×3 identity matrix. Let $\boldsymbol{M} = \mathrm{diag}(m_1, m_2, m_3)$ and $\boldsymbol{J} = \mathrm{diag}(J_1, J_2, J_3)$. Furthermore, assume that $m_w = 0$ so that $\boldsymbol{r_s} = \boldsymbol{0}$. We can then compute the momenta as

$$\begin{pmatrix} \boldsymbol{P} \\ \boldsymbol{\Pi} \\ \boldsymbol{P_p} \end{pmatrix} = \begin{pmatrix} \partial T / \partial \boldsymbol{v} \\ \partial T / \partial \boldsymbol{\Omega} \\ \partial T / \partial \dot{\boldsymbol{r}}_{\boldsymbol{p}} \end{pmatrix} = \boldsymbol{I} \begin{pmatrix} \boldsymbol{v} \\ \boldsymbol{\Omega} \\ \dot{\boldsymbol{r}}_{\boldsymbol{p}} \end{pmatrix} \tag{3.9}$$

$$=: \begin{pmatrix} \boldsymbol{M}+\bar{m}\boldsymbol{\mathcal{I}} & -\bar{m}\hat{\boldsymbol{r}}_{\boldsymbol{p}} & \bar{m}\boldsymbol{\mathcal{I}} \\ \bar{m}\hat{\boldsymbol{r}}_{\boldsymbol{p}} & \boldsymbol{J}-\bar{m}\hat{\boldsymbol{r}}_{\boldsymbol{p}}\hat{\boldsymbol{r}}_{\boldsymbol{p}} & \bar{m}\hat{\boldsymbol{r}}_{\boldsymbol{p}} \\ \bar{m}\boldsymbol{\mathcal{I}} & -\bar{m}\hat{\boldsymbol{r}}_{\boldsymbol{p}} & \bar{m}\boldsymbol{\mathcal{I}} \end{pmatrix} \begin{pmatrix} \boldsymbol{v} \\ \boldsymbol{\Omega} \\ \dot{\boldsymbol{r}}_{\boldsymbol{p}} \end{pmatrix}.$$

Inverting these relationships then gives the body velocities in terms of the body momenta. To get the equations of motion in terms of body velocities, we differentiate the equation for the body velocities with respect to time. We assume that buoyancy is changed in a symmetric way (e.g., ballast is pumped on and off board in streams with the appropriate symmetry) so that there is negligible associated thrust or moment on the glider. Let the ballast control input u_4 be defined as

$$u_4 = \dot{m}_b \ . \tag{3.10}$$

Differentiating the body velocities $\boldsymbol{v}$, $\boldsymbol{\Omega}$, and $\dot{\boldsymbol{r}}_{\boldsymbol{p}}$, then substituting for the derivatives $\dot{\boldsymbol{P}}$, $\dot{\boldsymbol{\Pi}}$ and $\dot{\boldsymbol{P}}_{\boldsymbol{p}}$, and substituting (3.9) for the relationship between momenta and velocity, the complete equations of motion for the underwater glider moving in three-dimensional space are

$$\begin{pmatrix} \dot{\boldsymbol{R}} \\ \dot{\boldsymbol{b}} \\ \dot{\boldsymbol{\Omega}} \\ \dot{\boldsymbol{v}} \\ \dot{\boldsymbol{r}}_{\boldsymbol{p}} \\ \dot{\boldsymbol{P}}_{\boldsymbol{p}} \\ \dot{m}_b \end{pmatrix} = \begin{pmatrix} \boldsymbol{R}\hat{\boldsymbol{\Omega}} \\ \boldsymbol{R}\boldsymbol{v} \\ \boldsymbol{J}^{-1}\bar{\boldsymbol{T}} \\ \boldsymbol{M}^{-1}\bar{\boldsymbol{F}} \\ \frac{1}{\bar{m}}\boldsymbol{P}_{\boldsymbol{p}} - \boldsymbol{v} - \boldsymbol{\Omega}\times\boldsymbol{r}_{\boldsymbol{p}} \\ \bar{\boldsymbol{u}} \\ u_4 \end{pmatrix}, \tag{3.11}$$

$$\begin{aligned} \bar{\boldsymbol{T}} &= (\boldsymbol{J}\boldsymbol{\Omega} + \hat{\boldsymbol{r}}_p\boldsymbol{P}_{\boldsymbol{p}})\times\boldsymbol{\Omega} + \boldsymbol{M}\boldsymbol{v}\times\boldsymbol{v} + \bar{m}g\hat{\boldsymbol{r}}_{\boldsymbol{p}}\boldsymbol{R}^{\boldsymbol{T}}\boldsymbol{k} \\ &\quad + \boldsymbol{T}_{\boldsymbol{ext}} - \hat{\boldsymbol{r}}_{\boldsymbol{p}}\bar{\boldsymbol{u}} \\ \bar{\boldsymbol{F}} &= (\boldsymbol{M}\boldsymbol{v} + \boldsymbol{P}_{\boldsymbol{p}})\times\boldsymbol{\Omega} + m_0g\boldsymbol{R}^{\boldsymbol{T}}\boldsymbol{k} + \boldsymbol{F}_{\boldsymbol{ext}} - \bar{\boldsymbol{u}}. \end{aligned}$$

Here,

$$\begin{aligned} \boldsymbol{F}_{\boldsymbol{ext}} &= \boldsymbol{R}^{\boldsymbol{T}}\sum \boldsymbol{f}_{\boldsymbol{ext_i}} \ , \\ \boldsymbol{T}_{\boldsymbol{ext}} &= \boldsymbol{R}^{\boldsymbol{T}}\sum(\boldsymbol{x_i}-\boldsymbol{b})\times\boldsymbol{f}_{\boldsymbol{ext_i}} + \boldsymbol{R}^{\boldsymbol{T}}\sum\boldsymbol{\tau}_{\boldsymbol{ext_j}} \ , \end{aligned}$$

refer to external forces and moments, in this case lift and drag, with respect to the body frame.

3.2 Equations of Motion in the Vertical Plane

We now specialize the model to the vertical plane, the $\boldsymbol{i}$-$\boldsymbol{k}$ plane in inertial coordinates and the $\boldsymbol{e_1}$-$\boldsymbol{e_3}$ plane in body coordinates. The elements of $\boldsymbol{R}$, $\boldsymbol{b}$, $\boldsymbol{v}$, $\boldsymbol{\Omega}$, $\boldsymbol{r_p}$, $\boldsymbol{P_p}$, and $\bar{\boldsymbol{u}}$ corresponding to the $\boldsymbol{e_2}$ direction are set to zero. The equations of motion (3.11) for the gliding vehicle restricted to the vertical plane are then

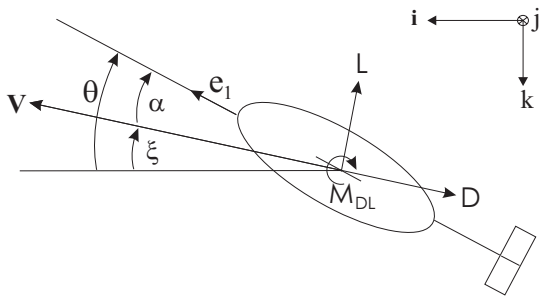

Figure 3.4: Lift and drag on glider.

$$\begin{aligned}
\dot{x} &= v_1\cos\theta + v_3\sin\theta && (3.12)\\
\dot{z} &= -v_1\sin\theta + v_3\cos\theta && (3.13)\\
\dot{\theta} &= \Omega_2 && (3.14)\\
\dot{\Omega}_2 &= \frac{1}{J_2}((m_3-m_1)v_1v_3 && (3.15)\\
&\quad -\bar{m}g(r_{P1}\cos\theta + r_{P3}\sin\theta) \\
&\quad +M_{DL} - r_{P3}u_1 + r_{P1}u_3) \\
\dot{v}_1 &= \frac{1}{m_1}(-m_3v_3\Omega_2 - P_{P3}\Omega_2 - m_0g\sin\theta \\
&\quad +L\sin\alpha - D\cos\alpha - u_1) && (3.16)\\
\dot{v}_3 &= \frac{1}{m_3}(m_1v_1\Omega_2 + P_{P1}\Omega_2 + m_0g\cos\theta \\
&\quad -L\cos\alpha - D\sin\alpha - u_3) && (3.17)\\
\dot{r}_{P1} &= \frac{1}{\bar{m}}P_{P1} - v_1 - r_{P3}\Omega_2 && (3.18)\\
\dot{r}_{P3} &= \frac{1}{\bar{m}}P_{P3} - v_3 + r_{P1}\Omega_2 && (3.19)\\
\dot{P}_{P1} &= u_1 && (3.20)\\
\dot{P}_{P3} &= u_3 && (3.21)\\
\dot{m}_b &= u_4 && (3.22)
\end{aligned}$$

Here, θ is pitch angle, α is the angle of attack, D is drag, L is lift and M_{DL} is the viscous moment as shown in Figure 3.4. These forces and moment are modelled as

$$\begin{aligned} D &= (K_{D_0} + K_D\alpha^2)(v_1^2+v_3^2) \\ L &= (K_{L_0} + K_L\alpha)(v_1^2+v_3^2) \\ M_{DL} &= (K_{M_0} + K_M\alpha)(v_1^2+v_3^2) \end{aligned}$$

where the K's are constant coefficients. This model is a standard one, derived using airfoil theory and potential flow calculations and then verified using experimental observations, see for example [4, 11]. The method for determination of the coefficients is described in Section 4.3.

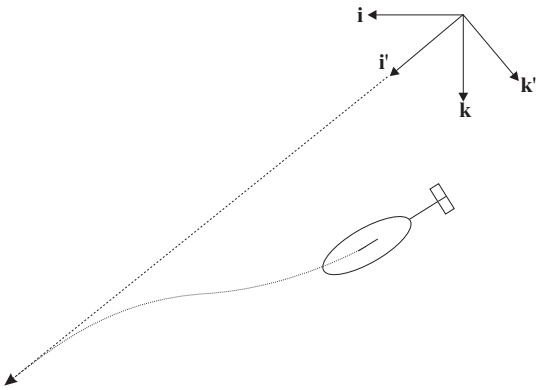

Figure 3.5: Planar gliding controlled to a line.

As shown in Figure 3.4, we denote the glide path angle by ξ where

$$\xi = \theta - \alpha.$$

We also denote the glider speed by V where

$$V = \sqrt{(v_1^2 + v_3^2)}.$$

We will typically specify a glide path by desired glide path angle ξ_d and desired speed V_d. We define inertial coordinates (x', z') such that x' coincides with the desired path:

$$\begin{pmatrix} x' \\ z' \end{pmatrix} = \begin{pmatrix} \cos\xi_d & -\sin\xi_d \\ \sin\xi_d & \cos\xi_d \end{pmatrix} \begin{pmatrix} x \\ z \end{pmatrix}. \quad (3.23)$$

Then, z' measures the vehicle's perpendicular distance to the desired path. We define two gliding objectives:

GO1 The objective is to control only the direction and speed of the vehicle's glide path. In this case we need not consider x and z at all.

GO2 The objective is to control gliding along a prescribed line (see Figure 3.5). In this case we will include z' (but exclude x') in our analysis and we aim to make $z' = 0$.

The dynamics of the z' state are

$$\begin{aligned} \dot{z}' &= \sin\xi_d(v_1\cos\theta + v_3\sin\theta) \quad (3.24) \\ &\quad + \cos\xi_d(-v_1\sin\theta + v_3\cos\theta). \end{aligned}$$

In several glider designs the moving mass is restricted to one degree of freedom in the planar case. This case is addressed in [10].

4 Controllability of Steady Glide Paths

In this section we compute steady glide paths. We then study controllability and observability of these glide paths.

4.1 Gliding Equilibria

We prescribe a desired glide path by specifying the desired glide path angle ξ_d and the desired speed V_d. We denote with subscript "d" the value of all dynamic variables at the glide equilibria. To get the conditions for such planar gliding equilibria, we set the left hand side of equations (3.24) and (3.14) through (3.22) to zero.

With their left hand sides set to zero and given ξ_d, equations (3.16) and (3.17) may be solved for α_d. We can then compute

$$\theta_d = \xi_d + \alpha_d, \quad v_{1_d} = V_d\cos\alpha_d, \quad v_{3_d} = V_d\sin\alpha_d,$$
$$P_{P1_d} = \bar{m}v_{1_d}, \quad P_{P3_d} = \bar{m}v_{3_d}.$$

m_{b_d} can then be solved again using (3.16) and (3.17). Finally, equation (3.15) with left hand side set to zero gives a one-parameter family of solutions for $(r_{P1_d}, r_{P3_d})^T$.

First, we compute α_d from equations (3.16) and (3.17) with left hand sides zero. This yields a quadratic equation for α_d. Provided $V_d \neq 0$ and $\xi_d \neq \pm\frac{\pi}{2}$, we have

$$\alpha_d^2 + \frac{K_L}{K_D}\tan\xi_d\alpha_d + \frac{1}{K_D}(K_{D_0} + K_{L_0}\tan\xi_d) = 0. \quad (4.1)$$

Equation (4.1) may be solved for a realizable α_d provided the discriminant of the quadratic equation is greater than or equal to zero. Evaluating the condition on the discriminant in the range $(-\frac{\pi}{2}, \frac{\pi}{2})$ will give a range of possible glide path angles ξ_d depending on the glider hydrodynamic parameters. See [10]. Since the drag model is valid only at small angles of attack, we take α_d as the solution of (4.1) with smaller magnitude,

$$\begin{aligned} \alpha_d &= \frac{1}{2}\frac{K_L}{K_D}\tan\xi_d \times \quad (4.2) \\ &\quad \left(-1 + \sqrt{1 - 4\frac{K_D}{K_L^2}\cot\xi_d(K_{D_0}\cot\xi_d + K_{L_0})}\right). \end{aligned}$$

The special case of $\xi_d = \pm\frac{\pi}{2}$ is covered in [10].

We may determine m_{b_d} from (3.16) and (3.17),

$$\begin{aligned} m_{b_d} &= (m - m_h - \bar{m}) + \frac{1}{g}\left(-\sin\xi_d(K_{D_0} + K_D\alpha_d^2)\right. \\ &\quad \left. + \cos\xi_d(K_{L_0} + K_L\alpha_d)\right)V_d^2. \quad (4.3) \end{aligned}$$

Finally, we may solve for a one-parameter family of sliding mass locations $(r_{P1_d}, r_{P3_d})^T$ which satisfy equation (3.15). The family of solutions is

$$\boldsymbol{r_{Pd}} = \boldsymbol{r}^{\perp} + \gamma \begin{pmatrix} -\sin\theta_d \\ \cos\theta_d \end{pmatrix} \tag{4.4}$$

where

$$\begin{aligned} \boldsymbol{r}^{\perp} &= \frac{1}{\bar{m}g}\left((m_{f3} - m_{f1})v_{1_d} v_{3_d}\right. \\ &\quad \left. +(K_{M_0} + K_M \alpha_d)V_d^2\right) \begin{pmatrix} \cos\theta_d \\ \sin\theta_d \end{pmatrix} \end{aligned}$$

and where γ is a real number. The vector $\boldsymbol{r}^{\perp}$ is a particular solution of equation (3.15). Since $(-\sin\theta, \cos\theta)^T = (\boldsymbol{R^T k})$ is the direction of gravity in body coordinates, $\boldsymbol{r}^{\perp}$ is orthogonal to the direction of gravity and γ measures the vehicle's "bottom-heaviness" as shown in Figure 4.1.

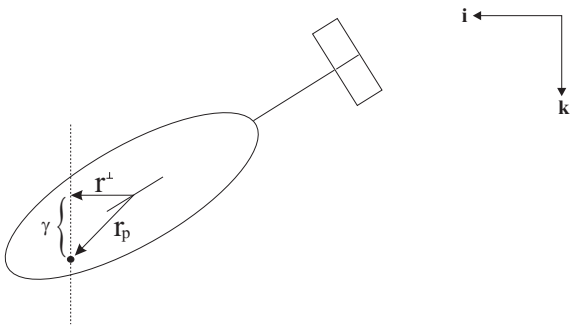

Figure 4.1: Family of possible movable mass locations for a steady glide.

For an experimental vehicle, r_{P3} may be a more physically relevant choice of parameter than γ. Equilibrium mass locations in this case are addressed in [10].

4.2 Linearization

We determine the linearization for the planar glider about a steady glide path. Let $\boldsymbol{x} = (z', \theta, \Omega_2, v_1, v_3, r_{p1}, r_{p3}, P_{P_1}, P_{P_3}, m_b)^T$ and let $\boldsymbol{u} = (u_1, u_3, u_4)^T$. Define

$$\begin{aligned} \boldsymbol{\delta x} &= \boldsymbol{x} - \boldsymbol{x_d} \\ \boldsymbol{\delta u} &= \boldsymbol{u} - \boldsymbol{u_d}. \end{aligned}$$

Then the linearized system is

$$\boldsymbol{\delta \dot{x}} = \boldsymbol{A}\ \boldsymbol{\delta x}\ +\ \boldsymbol{B}\ \boldsymbol{\delta u} \tag{4.5}$$

where

$$\boldsymbol{A} = \begin{bmatrix} 0 & -V_d & 0 & -\sin\alpha_d & \cos\alpha_d \\ 0 & 0 & 1 & 0 & 0 \\ 0 & a_{32} & 0 & a_{34} & a_{35} \\ 0 & a_{42} & a_{43} & a_{44} & a_{45} \\ 0 & a_{52} & a_{53} & a_{54} & a_{55} \\ 0 & 0 & -r_{P3} & -1 & 0 \\ 0 & 0 & r_{P1} & 0 & -1 \\ 0 & 0 & 0 & 0 & 0 \\ 0 & 0 & 0 & 0 & 0 \\ 0 & 0 & 0 & 0 & 0 \end{bmatrix}$$

$$\begin{bmatrix} 0 & 0 & 0 & 0 & 0 \\ 0 & 0 & 0 & 0 & 0 \\ -\frac{\bar{m}g\cos\theta_d}{J_2} & -\frac{\bar{m}g\sin\theta_d}{J_2} & 0 & 0 & 0 \\ 0 & 0 & 0 & 0 & a_{410} \\ 0 & 0 & 0 & 0 & a_{510} \\ 0 & 0 & \frac{1}{\bar{m}} & 0 & 0 \\ 0 & 0 & 0 & \frac{1}{\bar{m}} & 0 \\ 0 & 0 & 0 & 0 & 0 \\ 0 & 0 & 0 & 0 & 0 \\ 0 & 0 & 0 & 0 & 0 \end{bmatrix} \tag{4.6}$$

and

$$\boldsymbol{B} = \begin{bmatrix} 0 & 0 & 0 \\ 0 & 0 & 0 \\ -\frac{r_{P3_d}}{J_2} & \frac{r_{P1_d}}{J_2} & 0 \\ -\frac{1}{m_{b_d}+m_h+m_{f1}} & 0 & 0 \\ 0 & -\frac{1}{m_{b_d}+m_h+m_{f3}} & 0 \\ 0 & 0 & 0 \\ 0 & 0 & 0 \\ 1 & 0 & 0 \\ 0 & 1 & 0 \\ 0 & 0 & 1 \end{bmatrix}. \tag{4.7}$$

Here,

$$\begin{aligned} \alpha_{v_1} &= -\frac{v_3}{V^2} \\ \alpha_{v_3} &= \frac{v_1}{V^2} \\ D_{v_1} &= (K_{D_0} + K_D\alpha^2)(2v_1) - 2K_D\alpha v_3 \\ D_{v_3} &= (K_{D_0} + K_D\alpha^2)(2v_3) + 2K_D\alpha v_1 \\ L_{v_1} &= (K_{L_0} + K_L\alpha)(2v_1) - K_L v_3 \\ L_{v_3} &= (K_{L_0} + K_L\alpha)(2v_3) + K_L v_1 \\ M_{v_1} &= (K_{M_0} + K_M\alpha)(2v_1) - K_M v_3 \\ M_{v_3} &= (K_{M_0} + K_M\alpha)(2v_3) + K_M v_1 \end{aligned}$$

where we have abbreviated $\frac{\partial \alpha}{\partial v_1}$ as α_{v_1}, etc. and

$$
\begin{aligned}
a_{32} &= \frac{\bar{m}g}{J_2}(r_{P1_d}\sin\theta_d - r_{P3_d}\cos\theta_d) = \frac{\bar{m}g}{J_2}(-\gamma) \\
a_{34} &= \frac{1}{J_2}\left((m_{f3}-m_{f1})v_{3_d} + M_{v_1}|_{eq}\right) \\
a_{35} &= \frac{1}{J_2}\left((m_{f3}-m_{f1})v_{1_d} + M_{v_3}|_{eq}\right) \\
a_{42} &= -\frac{m_{0_d}}{m_{1_d}}g\cos\theta_d \\
a_{43} &= -\frac{m_{3_d}+\bar{m}}{m_{1_d}}v_{3_d} \\
a_{44} &= \frac{1}{m_{1_d}}\left(L_{v_1}\sin\alpha + L\cos\alpha\alpha_{v_1}\right. \\
&\quad \left. -D_{v_1}\cos\alpha + D\sin\alpha\alpha_{v_1}\right)_{eq} \\
a_{45} &= \frac{1}{m_{1_d}}\left(L_{v_3}\sin\alpha + L\cos\alpha\alpha_{v_3}\right. \\
&\quad \left. -D_{v_3}\cos\alpha + D\sin\alpha\alpha_{v_3}\right)_{eq} \\
a_{410} &= -\frac{g\sin\theta_d}{m_{1_d}} \\
a_{52} &= -\frac{m_{0_d}}{m_{3_d}}g\sin\theta_d \\
a_{53} &= \frac{m_{1_d}+\bar{m}}{m_{3_d}}v_{1_d} \\
a_{54} &= \frac{1}{m_{3_d}}\left(-L_{v_1}\cos\alpha + L\sin\alpha\alpha_{v_1}\right. \\
&\quad \left. -D_{v_1}\sin\alpha - D\cos\alpha\alpha_{v_1}\right)_{eq} \\
a_{55} &= \frac{1}{m_{3_d}}\left(-L_{v_3}\cos\alpha + L\sin\alpha\alpha_{v_3}\right. \\
&\quad \left. -D_{v_3}\sin\alpha - D\cos\alpha\alpha_{v_3}\right)_{eq} \\
a_{510} &= \frac{g\cos\theta_d}{m_{3_d}}
\end{aligned}
$$

The notation $(\cdot)|_{eq}$ indicates that the quantity is to be evaluated at the desired equilibrium.

4.3 Controllability

In this section we describe controllability and observabililty of steady glide paths for a model of our experimental vehicle ROGUE, described in Section 2. Mass and inertia properties were measured directly. Added mass and inertia properties can be found, for example, in [7]. Lift and drag for the body were found experimentally as described in [6]. Lift and drag for the wings were taken from the data in [13]. Lift for the body plus wings was then computed using Schrenk's method [12], and drag was computed as the sum of the drag on the wing and the body. The lift moment was approximated by taking into account the tail. The vehicle model parameters are given as follows:

$$
\begin{aligned}
m &= 11.22 \text{ kg} \\
m_h &= 8.22 \text{ kg} \\
\bar{m} &= 2.0 \text{ kg} \\
m_{f1} &= 2 \text{ kg} \\
m_{f3} &= 14 \text{ kg} \\
J_2 &= 0.1 \text{ Nm}^2 \\
K_{D_0} &= 18 \text{ N(s/m)}^2 \\
K_D &= 109 \text{ N(s/m)}^2 \\
K_L &= 306 \text{ N(s/m)}^2 \\
K_M &= -36.5 \text{ Nm(s/m)}^2.
\end{aligned}
$$

The first three masses, m, m_h and $\bar{m}$ were measured with a high degree of accuracy. The other terms have less precision because they are based on look-up tables and approximation methods.

Four steady glide paths are calculated using the method of Section 4.1. The glide paths are at glide angles $-30°$, $-45°$, $30°$ and $45°$. We compute the glide path at $-30°$ by choosing a desired glide speed $V_d = 0.30$ m/s and a desired vertical location of the movable mass given by $r_{P3_d} = 4$ cm. This results in an equilibrium variable mass given by $m_{b_d} = 1.36$ kg. The glide path at $-45°$ is computed for these same values of r_{P3_d} and m_{b_d}. The corresponding equilibrium speed for this glide is computed as $V_d = .37$ m/s. Similarly, we computed the two steady upward glide paths, for the same value of r_{P3_d} and the same buoyant force magnitude, i.e., the value of $|m_{0_d}|$ is held constant. Recall that m_0 is the mass of the vehicle m_v less the mass of the displaced fluid m. The full description of each of the four glide paths is given in Table 4.1.

Variable	Down 30°	Down 45°	Up 30°	Up 45°
ξ_d (deg)	-30	-45	30	45
θ_d (deg)	-23.7	-41.5	23.7	41.5
α_d (deg)	6.3	3.5	-6.3	-3.5
V_d (m/s)	0.30	0.37	0.30	0.37
v_{1_d} (m/s)	0.29	0.36	0.29	0.36
v_{3_d} (m/s)	0.03	0.02	-0.03	-0.02
r_{P1_d} (cm)	0.41	2.20	-0.41	-2.20
r_{P3_d} (cm)	4.0	4.0	4.0	4.0
P_{P1_d} (kg-m/s)	0.60	0.73	0.60	0.73
P_{P3_d} (kg-m/s)	0.07	0.04	-0.07	-0.04
m_{b_d} (kg)	1.36	1.36	0.64	0.64
m_{0_d}(kg)	0.36	0.36	-0.36	-0.36

Table 4.1: Four Steady Glide Paths for ROGUE

Local properties of these steady glide paths can be studied using the linearization of Section 4.2. By

plugging in the equilibrium values, we can examine the linearization for stability, controllability and observability. The four glide paths listed in Table 4.1 all have a relatively slow unstable mode. They are all, however, locally controllable. That is, $\boldsymbol{A}$ and $\boldsymbol{B}$ as given by (4.6) and (4.7), when evaluated at any of the four equilibria, satisfy the controllability rank condition. Note that the linearization includes the state z' meaning that controllability extends to the variable z'. Accordingly, we can successfully design a linear controller that will locally accomplish not only glide objective **GO1** but also **GO2**.

It is of interest to check the controllability rank condition in the case that the movable mass $\bar{m}$ can only move in one direction (i.e., r_{P3} is fixed). To do this we have linearized the equations of motion for the single degree-of-freedom moving mass derived in [10]. Again the new $\boldsymbol{A}$ and $\boldsymbol{B}$ matrices for this case, when evaluated at any of the above four glide paths, satisfy the controllability rank condition. Thus, it seems that at least for linear type control action, not much is lost in restricting the degrees of freedom of the movable mass from two to one. Several operational gliders have moving masses that translate in the vehicle long axis and rotate in the roll direction, corresponding to a design with one degree of freedom when considering only the vertical plane.

The movable mass $\bar{m}$ for ROGUE is approximately $1/6$ of the vehicle displacement m. This is of the same relative order as the movable mass in the gliders SLOCUM, Spray and Seaglider. Variations in this mass or its location will not in principle affect local controllability of a feasible glide path, but may affect the range of feasible glide paths and the switching between them.

4.4 Observability and State Estimation

Observability of the linearized model about the four glide paths listed in Table 4.1 was also investigated. If **GO1** is our objective, i.e., if we are interested in controlling only the direction and speed of the vehicle's glide path, then we need not measure z'. The nine-dimensional dynamic model (which excludes z') is completely observable with measurements limited to movable mass position r_{p1}, r_{p3} and variable mass m_b. In this case, pitch angle θ, pitch rate Ω_2, linear velocity components v_1 and v_3 and the momentum of the movable mass P_{p1}, P_{p3} need not be sensed. Observability means that with the measurements of r_{p1}, r_{p3} and m_b, a dynamic observer could be designed to give an estimate of the unmeasured states θ, Ω_2, v_1, v_3, P_{p1} and P_{p3}. Of course, θ is typically already measured and Ω_2 is not so hard to measure, so the real advantage is in the estimation of v_1, v_3, P_{p1} and P_{p3} which are more difficult to measure. The nine-dimensional dynamic model is also completely observable with measurements limited to θ, r_{p1} (or r_{p3}) and m_b. Again this means that using these three measurement signals, an observer could be designed to estimate the rest of the states.

We note that the use of a dynamic observer to estimate the glider states has the potential to improve the accuracy of horizontal motion determination over current methods which are based on assumptions of constant angle of attack, etc. For example, on SLOCUM, the horizontal motion of the glider during the glide is estimated from GPS fixes taken at the surface, measured pitch angle θ, an assumed angle of attack and vertical speed computed from depth measurements [17]. Similarly, on Spray, horizontal flight distance is calculated based on a constant pitch, heading and angle of attack to which the vehicle is being controlled [14].

If **GO2** is our objective, i.e., if we want to control the glider to a prescribed line in the plane, then we need a measurement of z'. Recall from (3.23) that z' depends on both depth z, which is easily measured, and horizontal position x, which is not so easily measured. The measurements r_{p1}, r_{p3} and m_b, together with a measurement of z (or alternatively θ, r_{p1}, m_b and z), do not render x observable. This means that without an initial condition measurement $x(0)$, the trajectory $x(t)$ cannot be computed,and so z' is not observable. That is, using any combination of the other nine states, it is not possible to design a dynamic observer to estimate the z' state. However, with an initial measurement of x given say from a GPS fix taken when the glider is at the surface, the horizontal motion of the glider can be dead reckoned using velocity estimates from the observer. This introduces some error $z' - z'_{ded}$ into the estimate of the z' state. Using the deduced z'_{ded} in the feedback control, the glider can perform **GO2**, gliding along or parallel to the desired glide path with some offset in the z' direction due to dead reckoning error.

The dead reckoning approach involves calculating horizontal velocity $\dot{x}_{ded}$, then integrating to obtain a deduced x_{ded}.

$$\dot{x}_{ded} \quad = \quad v_{1est}\cos\theta + v_{3est}\sin\theta. \qquad (4.8)$$

This can then be used to calculate z'_{ded}. The pitch angle θ and depth z can be measured directly. Estimates of the velocities, v_{1est} and v_{3est}, are provided by the observer, while ξ_d is determined by the de-

sired glide. The equation for the dead reckoned z'_{ded} is then

$$z'_{ded} = \sin\xi_d(x_{ded}) + \cos\xi_d(z). \quad (4.9)$$

The nine observable states include v_1 and v_3 so our observer estimates v_{1est} and v_{3est} will converge to the actual states when we are close enough to the equilibrium glide path for the linearization to be valid. When there is some error in the observer estimate of the velocities, integrating (4.8) to find x_{ded} and using (4.9) will result in some error $z' - z'_{ded} \neq 0$. This error depends on the observer state estimate error, which will vary with different state trajectories and disturbances.

5 Controlled Planar Gliding With Observer

In this section we demonstrate, in simulation, controlled gliding in the vertical plane by designing and testing a linear controller and observer for the glide path moving 30° downward as described in Table 4.1. Since the controller is linear, we expect that it should take initial conditions nearby to the 30° downward glide path. We demonstrate this result by starting the glider at the 45° downward steady glide and using the linear controller to move it to the 30° downward glide solely by feedback.

5.1 Controller Design

We address the case where only a limited set of the states are measured, depending on the sensors on the glider. We design the controller and then, given the limited set of state measurements, design a dynamic observer to determine the full state of the glider. The controller is designed for the linearization about the 30° downward glide using the LQR (linear quadratic regulator) method. This is a standard linear optimal control design method which produces a stabilizing control law that minimizes a cost function that is a weighted sum of the squares of the states and input variables.

The cost function to be minimized is defined as

$$J = \int_0^\infty \boldsymbol{\delta x^T Q \delta x + \delta u^T R \delta u}\, dt$$

where $\boldsymbol{Q}$ and $\boldsymbol{R}$ are state and control penalty matrices. $\boldsymbol{Q}$ and $\boldsymbol{R}$ were chosen to ensure well-behaved dynamics and to prevent large motions in the movable mass position and variable mass that would exceed physical limitations. Taking into account real or desirable maximum state values, the states associated with vehicle and movable mass velocity and variable mass and pitch angle were weighted most heavily. No significant tuning was performed. The weight selections are given by

$$\begin{aligned} \boldsymbol{Q} &= \text{diag}(.05, .5, 1, 2, 2, .1, .1, 1, 1, .5), \\ \boldsymbol{R} &= \text{diag}(1, 1, 1). \end{aligned}$$

The corresponding control law is $\boldsymbol{u = -K\delta x}$ where $\boldsymbol{K}$ is computed using MATLAB as the solution to the Riccati equation given $\boldsymbol{A, B, Q, R}$.

5.2 Observer Design

In the case that some states are not provided by sensor data, as is likely to be the case with velocities v_1 and v_3 in an autonomous glider, it is possible to construct a linear optimal observer to estimate the unavailable states. As described in Section 4.3 the nine dimensional dynamic model excluding z' is completely observable. If z' is not directly sensed, it is an unobservable state but can be dead reckoned. The construction of an optimal linear observer for the nine dimensional system proceeds in a similar manner to the construction of the LQR controller.

Our linear system is described by $\boldsymbol{A}$ and $\boldsymbol{B}$, defined above. The system output is $\boldsymbol{y = Cx + v}$, where $\boldsymbol{C}$ is the system output matrix determined by the available sensors and $\boldsymbol{v}$ is noise. Given a linear time invariant system subject to additive process disturbance $\boldsymbol{w(t)}$ and measurement noise $\boldsymbol{v(t)}$ which are zero mean, gaussian, white noise processes, an observer which minimizes variance in the estimate error is derived in a manner similar to the LQR. The cost function to be minimized is

$$J_0 = \int_0^\infty [\tilde{z}_w(t)^2 + \tilde{z}_v(t)^2]\, dt$$

where $\tilde{z}_w(t) = e^{(\boldsymbol{A-LC})t}\boldsymbol{w_0}$ is the system zero-state response to plant disturbance $\boldsymbol{w(t) = w_0}u_0(t)$ and $\tilde{z}_v(t) = -e^{(\boldsymbol{A-LC})t}\boldsymbol{Lv_0}$ is the zero-state response to measurement noise $\boldsymbol{v(t) = v_0}u_0(t)$. Let $\boldsymbol{w(t)} = \boldsymbol{w_0}\delta(t)$ and $\boldsymbol{v(t)} = \boldsymbol{v_0}\delta(t)$ represent the white-noise processes $\boldsymbol{w(t)}$ and $\boldsymbol{v(t)}$, where the Dirac Delta Function $\delta(t)$ represents the fact that white noise is uncorrelated in time. Let $\boldsymbol{W} = \boldsymbol{w_0 w_0}^T$ and $\boldsymbol{V} = \boldsymbol{v_0 v_0}^T$ be the disturbance and noise covariance matrices. Then choosing observer feedback $\boldsymbol{L = PC^T V^{-1}}$ minimizes the cost function J_0, where $\boldsymbol{P}$ is the solution to the observer matrix Riccati equation given $\boldsymbol{A, C, W, V}$.

In this observer design the $\boldsymbol{W}$ and $\boldsymbol{V}$ matrices are chosen according to reasonable estimates of the

disturbances and noise. The covariance matrix $\boldsymbol{W}$ is a diagonal matrix whose elements are the square of the standard deviation of the state disturbances. The standard deviation is taken to be ten percent of the desired value at the equilibrium glide for each state. In the cases where a state $\boldsymbol{x}_i$ has desired value zero, we determined a maximum deviation $\triangle \boldsymbol{x}_i$ from equilibrium by simulating several switches between equilibrium glides under full state feedback control. Ten percent of $\triangle \boldsymbol{x}_i$ is then used as the standard deviation for the i^{th} state. The noise covariance matrix $\boldsymbol{V}$ depends on the noise properties of the sensors used in the vehicle. In this design they are taken to be of the same or smaller order of magnitude as $\boldsymbol{W}$:

$$\begin{aligned} \boldsymbol{W} &= \text{diag}(17, 4, 9, 1, 1, 1, 6, 0, 5), \\ \boldsymbol{V} &= \text{diag}(1, 1, 1, 1, 1). \end{aligned}$$

When determining the cost function to be minimized, if $\boldsymbol{V}$ is large then computed gain $\boldsymbol{L}$ will be small, so direct measurements have smaller impact on the state estimate. A large $\boldsymbol{W}$ implies disturbances dominate the plant dynamics. In that case computed gain $\boldsymbol{L}$ is large, resulting in an observer state estimate which depends more heavily on sensor measurements than the plant model.

5.3 Glider Simulation

In Figures 5.1-5.3 we show a MATLAB simulation of the glider switching from a 45° downward glide to a 30° downward glide path. This is accomplished by turning off the controller for the first glide at $t = 5$ seconds and turning on the linear controller for the second glide. In each figure we show results using full state feedback and using an observer to estimate the state used in the control law.

When calculating the controller gain matrix $\boldsymbol{K}$ and the observer gain matrix $\boldsymbol{L}$, some plant parameter error is incorporated into the design. When calculating the gain matrices using the respective Riccati equations, the parameters which determine the $\boldsymbol{A}$ and $\boldsymbol{B}$ matrices are varied by up to ten percent. Changing the $\boldsymbol{A}$ and $\boldsymbol{B}$ matrices used as the system model in the controller and observer design represents imperfect knowledge of the glider dynamic coefficients.

In Figure 5.1 we show the glide path before and after the switch. In Figure 5.2 we show plots of position, pitch, linear and angular velocity as a function of time and in Figure 5.3 we show the position of the movable mass, the net buoyant force as well as the control inputs as a function of time. The figures show that the 45° downward glide path is in the region of attraction of the linear controller designed for the 30° downward glide path. Furthermore, the transient is well behaved.

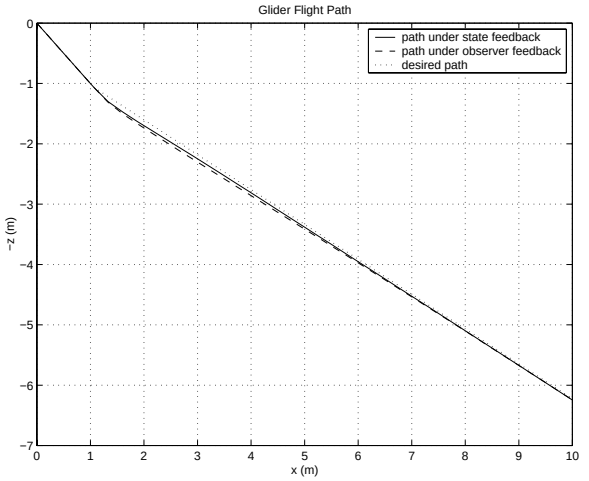

Figure 5.1: Simulation of glide path from 45° downward to 30° downward.

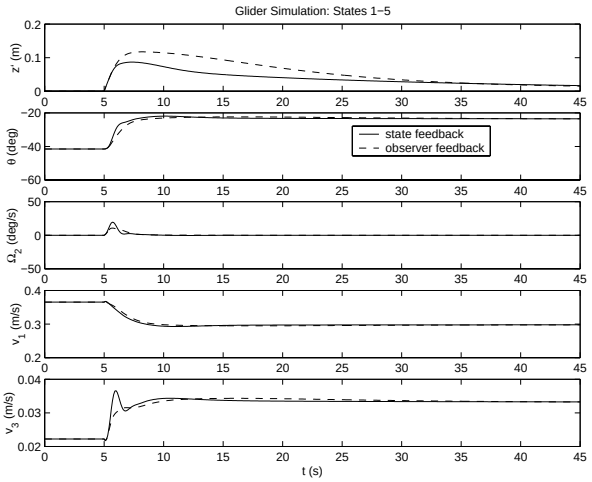

Figure 5.2: Simulation of position and velocity variables.

6 Final Remarks

Laboratory experiments of controlled gliding with ROGUE will be described in a future publication. Experiments with ROGUE are planned to provide verification of our dynamic model and to test the controller and observer designs. We also plan to realize these and future results on sea-worthy gliders

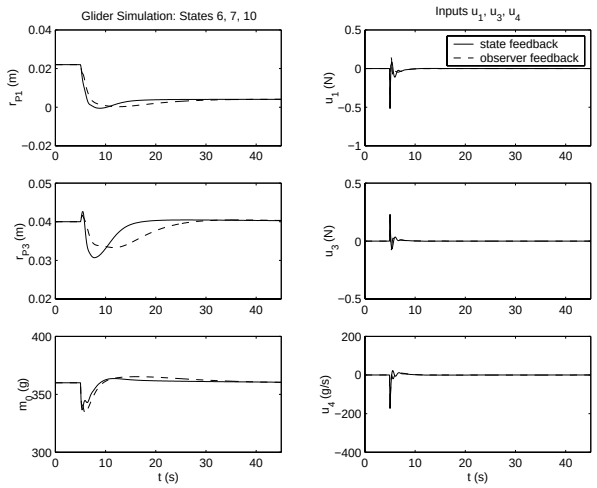

Figure 5.3: Simulation of movable mass, variable mass and control inputs.

such SLOCUM in collaboration with our colleagues who build and operate these vehicles.

Other future work includes extending the glider control design to motions in the horizontal plane such as waypoint following, control of unsteady motions, and three dimensional motions such as gliding in a spiral. We intend to develop the glider control methodology further by investigating nonlinear feedback control laws, feedforward control and path planning. Work with colleagues on optimal control theory which is applicable to glider path planning appears in [2].

Work is underway to develop decentralized control laws to produce underwater vehicles that school like fish [9, 15]. By developing control schemes for coordinated group motion of underwater vehicles, we hope to produce a network of gliders that can serve as a fast and effective ocean sensing platform. For example, in [1], decentralized control algorithms are described that allow a pair of vehicles to climb a spatially distributed gradient. In support of this effort we are building an experimental, underwater test-bed for multiple-vehicle control [1]. Vehicle systems, including control systems, hardware and software, and new sensors developed for the experimental grouping vehicle in [1] may also be incorporated into the design of future laboratory gliders.

7 Acknowledgements

We would like to thank Monique Chyba, Kristin Pettersen, Ralf Bachmayer and Craig Woolsey for helpful discussions on this work.

References

[1] R. Bachmayer and N.E. Leonard. Experimental test-bed for multi-vehicle control, navigation and communication. In *Proc. 12th Int. Symposium on Unmanned Untethered Submersible Tech.*, Durham, NH, 2001. To appear.

[2] M. Chyba, N.E. Leonard, and E.D Sontag. Optimality for underwater vehicles. In *Proc. IEEE Conference on Decision and Control*, 2001. To appear.

[3] C. C. Eriksen, T. J. Osse, T. Light, R. D. Wen, T. W. Lehmann, P. L. Sabin, J. W. Ballard, and A. M. Chiodi. Seaglider: A long range autonomous underwater vehicle for oceanographic research. *IEEE Journal of Oceanic Engineering, Special Issue on Autonomous Ocean Sampling Networks*, 2001. In press.

[4] Bernard Etkin. *Dynamics of Flight.* John Wiley and Sons, New York and London, 1959.

[5] H. Goldstein. *Classical Mechanics.* Addison-Wesley, 1980. 2nd edition.

[6] J.G. Graver, J. Liu, C. Woolsey, and N. E. Leonard. Design and analysis of an underwater vehicle for controlled gliding. In *Proc. 32nd Conference on Information Sciences and Systems, Princeton.*, pages 801–806, 1998.

[7] I. A. Kibel, N. E. Kochen, and N. V. Roze. *Theoretical Hydromechanics.* Wiley, 1964.

[8] H. Lamb. *Hydrodynamics.* Dover, New York, 6th edition, 1932.

[9] N.E. Leonard and E. Fiorelli. Virtual leaders, artificial potentials and coordinated control of groups. In *Proc. IEEE Conference on Decision and Control*, 2001. To appear.

[10] N.E. Leonard and J.G. Graver. Model-based feedback control of autonomous underwater gliders. *IEEE Journal of Oceanic Engineering, Special Issue on Autonomous Ocean Sampling Networks*, 2001. In press.

[11] B. W. McCormick. *Aerodynamics, Aeronautics and Flight Mechanics.* John Wiley, New York and London, 1979.

[12] O. Schrenk. A simple approximation method for obtaining spanwise lift distribution. Technical report, NACA, 1940.

[13] M. S. Selig, J. F. Donovan, and D. B. Fraser. *Airfoils at Low Speeds*. H. A. Stokely, Virginia Beach, VA, 1989.

[14] J. Sherman, R. E. Davis, W. B. Owens, and J. Valdes. The autonomous underwater glider 'Spray'. *IEEE Journal of Oceanic Engineering, Special Issue on Autonomous Ocean Sampling Networks*, 2001. In press.

[15] T.R. Smith, H. Hanßmann, and N.E. Leonard. Orientation control of multiple underwater vehicles with symmetry-breaking potentials. In *Proc. IEEE Conference on Decision and Control*, 2001. To appear.

[16] H. Stommel. The Slocum mission. *Oceanography*, 2:22–25, 1989.

[17] D. Webb and C. Jones. Personal communication, 2001.

[18] D. C. Webb, P. J. Simonetti, and C.P. Jones. SLOCUM, an underwater glider propelled by environmental energy. *IEEE Journal of Oceanic Engineering, Special Issue on Autonomous Ocean Sampling Networks*, 2001. In press.